Chapter 2

Improvement of Field-Emission Characteristics of Carbon Nanotube Field- Emission-Arrays by Oxide Capping Layer

The density distribution of CNTs is one of the crucial parameters dominating the field-emission characteristics of CNTs. To effectively control the density of CNTs, an oxide capping layer is deposited on a catalyst. The results show that improved field emission property can be obtained with a thin SiO_x layer on the catalyst layer as the precursor. Microwave plasma-enhanced chemical vapor deposition (MPCVD) and thermal chemical vapor deposition (TCVD) are used to grow nanotubes. For 3.5 nm Fe and 3.5 nm SiO_x on 3.5 nm Fe as catalysts to grow nanotubes in MPCVD, the turn-on field can be decreased from 3.7 V/μm. to 2.2 V/μm and the field-emission current density increases from $3.8x10^{-6}$ mA/cm^2 to $1.5x10^{-3}$ mA/cm^2 when the applied field was 3.5 V/μm. The threshold field which is defined as the field at which an emission current density of 10 mA/cm^2 is generated is about 5.32 V/μm. For 5 nm Fe and 1.5 nm SiO_x on 5 nm Fe as a catalyst to grow nanotubes in TCVD, the turn-on electric field reduced from 3.8 V/μm to 1.8 V/μm and the emission current density increased from 7×10^{-8} mA/cm^2 to $1.77mA/cm^2$ at an applied electric field of 3.5 V/μm.

2.1 Introduction

Carbon nanotubes have attracted considerable attention owing to their excellent electronic and structural properties, enabling their use in a broad range of applications [2.1-2.2]. Due to their high aspect ratio and small radii of curvature, carbon nanotubes can easily emit electrons at a very low electron field with respect to Si tips, coated Si tips, diamond or diamond-like carbon [2.3], and their chemical stability is excellent as well. Therefore, one of the most potential applications of carbon nanotubes is as the field emission material in vacuum microelectronics, such as flat- panel field-emission displays (FEDs), nanoprobes of atomic force microscopes (AFMs), microsensors, or scanning tunneling microscopes (STMs) and microsized intense electron sources [2.4-2.9]. The excellent field emission properties of carbon nanotubes have been demonstrated by several groups [2.10-2.16]. These groups have demonstrated the low turn-on electric field properties and extremely high emission current of CNT field-emission diodes. In most studies, arc-produced CNTs [2.14] and screen-printing techniques are used to fabricate low-cost CNT field-emission diodes for field-emission displays. However, specific purification processes for arc-produced CNTs are required, and the uniformity of screen-printed CNT field-emitter arrays is so poor that it results in a nonuniform emission current. The selective growth of CNTs by chemical vapor deposition (CVD) processes is sufficient for fabricating field-emission

devices with excellent uniformity when no purification or screen-printing process is required. However, the density of CNTs, which is an important parameter dominating field-emission property, cannot be controlled well by chemical vapor deposition processes such as laser ablation [2.15], thermal chemical vapor deposition [2.16-2.17], and microwave plasma-enhanced chemical vapor deposition (MPCVD) [2.18]. The screening of the electric field by the dense arrangement of CNTs has been reported by several groups [2.19-2.21]. The electric field is screened out for the closely spaced CNTs, which results in a reduced effective electric field near the CNT emitters. As a result, turn-on electric field increases and emission current density decreases. To obtain better field emission properties, the density of CNTs should be optimized. However, the density of CNTs synthesized by MPCVD and TCVD is very high and is difficult to control.

The density of the CNTs, dominating the field-emission properties, can be controlled by altering the thickness of the catalyst for the CNTs synthesized by the MPCVD and TCVD. In this study, a novel method for CNT growth with controlled density under low temperature was demonstrated. By applying an inactive layer (SiO) on the thin catalyst film, part of the catalyst can be covered as the formation of nanoparticles. The growth rate was thus varied for the covered and uncovered catalyst nanoparticles. A significant improvement in field-emission properties was observed

by oxide capping layer deposited on metal catalyst.

2.2 Experimental Procedure

The fabrication procedures of patterned CNT emitters are shown schematically in Figs. 2-1(a) ~2-1 (d). A 1-μm-thick photoresist was spin-coated on an n-type Si (100) substrate and square cells with a length of 1 mm (emission area is $1mm^2$) were defined by photolithography, as shown in Fig. 2-1(a). A catalytic iron layer was deposited directly on the photoresist-patterned Si substrate by sputtering. Afterward, a thin SiO_x film was deposited as the inactive layer, as shown in Fig. 2-1(b).Various thickness of SiO_x and Fe films were deposited to investigate the growth phenomenon and the field-emission properties of the CNT; the experimental parameters are shown in Table 2-1 and 2-3. The patterned precursor film was thus formed after the photoresist was removed by the lift-off method as depicted in Fig. 2-1(c). Finally, CNTs were grown selectively on the precursor by the MPCVD and TCVD system, respectively.

The growth condition of CNTs in the MPCVD system is listed as follows. H_2 plasma treatment was applied to the precursor films for 10 min before CNT growth, the gas flow rate was 80 sccm, and the chamber pressure is maintained at 35Torr, the microwave power was maintained at 1.2 kW. During CNT growth, CH_4, N_2 and H_2 are used as the source gases and their typical flow rates aree 20, 80, and 80sccm,

respectively. The microwave power is kept at 1.2 kw and the pressure is kept at 35 Torr.

The growth condition of CNTs in TCVD is listed as follows. Samples are placed horizontal up into the reactor at about 400°C, and then be heated to 700°C in pure N_2 with the flow rate at 1000 sccm. When the temperature is stabilized, N_2/H_2 mixture gases are fed into the furnace to pre-treat the catalytic film with the same gas flow rate at 500sccm for 10min. Finally, C_2H_4 at 20 sccm is added to the N_2/H_2 mixture gases for CNTs' growth. The gas pressure is held at about 1 atm and the growth time is 10 min.

Scanning electron microscopy (SEM) is performed to discover the morphology of the CNTs. The field-emission properties of the CNTs are characterized in a high-vacuum environment with a base pressure of 1.0×10^{-7} Torr. A schematic diagram of the apparatus is shown in Fig. 2-2. A glass plate coated with indium-tin oxide (ITO) and phosphor is positioned 100 μm (the electrode gap distance or spacer) above the sample surface as an anode. The emission current densities of the CNTs are measured as functions of applied electric field, using Keithley 237 high voltage units and an IEEE 488 interface controlled by a personal computer. The cathode luminescence can be obtained from the phosphor plate.

2.3 Results and Discussion

2.3.1 Effect of Oxide Capping layer on Field Emission Properties of Carbon Nanotubes Grown by Microwave Plasma Chemical Vapor Deposition

Figure 2-3 shows the morphology of the deposited CNTs with the precursor of 3.5 nm Fe. The length of the deposited CNTs is approximately 4 μm. The CNTs is aligned and closely spaced, and only a few of them protrude above the CNT surface. The flat top of the CNTs tends to result in the screening effect of the electric field during cold cathode operation. The field enhancement factor therefore decreases and the CNT emitter has poor field-emission properties. Alternatively, the electric field tends to be larger in the edge region that has a relatively low density of CNTs than in the center of the film. The non-uniform electric field distribution near the CNTs also affects the field-emission current distribution. The field-emission current emitted from the edge region of the CNT film as the applied field exceeded the turn-on electric field and the center part of the CNTs started to emit under a higher applied field. A schematic illustration is shown in Fig.2-4.

Figures 2-5(a) and 2-5(b) show SEM images of the deposited CNTs with the precursor of 3.5 nm/ 3.5 nm SiO_x/Fe. The CNT length decreased to approximately 3 μm and the arrangement of CNTs transferred from aligned and closely spaced to curved and randomly distributed. The random distribution of the CNTs results in a lower density, which is good for electric field distribution.

SEM images of the deposited CNTs with the precursor of 7.5nm SiO_x/3.5nm Fe are shown in Figs 2-6(a)-2-6(c). Figure 6(a) shows a low magnification SEM image of the deposited CNTs. High-magnification SEM image are shown in Figs. 2-6(b) and 2-6(c). Surprisingly, the deposited CNT film exhibited a bi-layered growth phenomenon. The CNTs grew upward from the substrate and downward from the SiO_x layer. The lengths of both groups of CNTs were approximately 6 μm.

Figure 2-7 shows the morphology of the deposited CNTs with the precursor of 15nm SiO_x/3.5nmFe. The low magnification SEM image shows that the CNTs only grew on the edge of the precursor. No nanotubes were found in the center part of the precursor from the morphologies of the CNTs shown.

The mechanisms of CNT grown are proposed. The growth mechanisms of the CNTs grown with different precursors are shown in Fig. 2-8. For the precursor of thin SiO_x film and thin Fe layer (3.5 nm and 3.5 nm, respectively), part of the SiO_x thin film was etched after the 10 min H_2 plasma pretreatment; the remaining of SiO_x film covered the Fe particles. During the CNT growth, the SiO_x-covered Fe particles were unable to absorb the carbon. However, the fast growth of CNTs occurred on the uncovered Fe film. As a result, the density of the carbon nanotubes decreased and the distribution of the nanotubes tended to be randomly distributed.

For the precursor with the thick SiO_x film and thin Fe layer (7.5 nm/ 3.5 nm SiO_x/Fe), we can observe that there still exists a thin inactive layer on top of the carbon nanotube film from the SEM images of Figs. 2-6(a)-2-6(c). The 7.5 nm SiO_x / 3.5 nm Fe precursor has a thinner SiO_x film after the CNT growth. Owing to the thinner SiO_x film, the loose structure of the SiO_x film (deposited by E-gun evaporation) and the high growth temperature (approximately 700°C), the carbon atoms should have a higher diffusive capability of penetrating the thinner inactive SiO_x layer. Therefore, during the nanotube growth, the carbon atoms can diffuse through the thin SiO_x layer and the interface between the precursor and Si substrate. The nanoparticles of the Fe started to absorb the carbon atoms, the carbon nanotubes were thus grown on the entire precursor region and lifted the SiO_x film and part of the Fe nanoparticles were adhered to it. The SiO_x-adhered Fe particles also absorbed carbon atoms and the nanotubes finally grew downward from the SiO_x film. However, in the case of 3.5 nm SiO_x / 3.5 nm Fe, no downward growth of nanotubes was observed. It is probable that the etched SiO_x layer almost disappears during nanotube growth, therefore none of the Fe nanoparticles can adhere to the SiO_x layer during downward nanotube growth.

In the case of the 15 nm SiO_x / 3.5 nm Fe precursor, the carbon atoms could not diffuse through the thick SiO_x layer. The carbon nanotubes were thus grown only in

the edge region of the patterned precursor film with the thick SiO_x film of 15 nm thickness.

Figure 2-9 (a) shows the field-emission properties of the deposited CNTs with the precursor of 3.5nm Fe, 3.5nm SiO_x on 3.5nm Fe, 7.5nm SiOx on 3.5nmFe nm and 15nm SiO_x on 3.5nm Fe. The corresponding F-N plots are shown in Fig. 2-9(b). The linearity of the F-N plot confirmed the field-emission phenomenon. The turn-on electric field of the CNTs grown with 3.5 nm Fe is 3.7 V/μm, and the turn-on field of the CNTs grown with 7.5 nm SiO_x on 3.5 nm Fe is 4 V/μm. The high turn-on field of the CNTs grown with 7.5 nm SiO_x on 3.5 nm Fe is attributed to the packed density of the nanotubes, moreover, the SiO_x-layer-covered CNTs are incapable of electron emission, the emission current density decreased from $1.6x10^{-1}$ mA/cm^2 to $5x10^{-2}$ mA/cm^2 under the applied field of 6 V/μm.

The turn-on field of the nanotubes grown with the precursor of 15 nm SiO_x on 3.5 nm Fe decreases from 3.7 V/μm. to 3.4 V/μm due to the reduced one-directional density of the nanotubes as compared with the CNTs grown without a SiO_x layer on Fe. However, the number of the emission sites decrease at the same time, and no significant improvement in field-emission current is obtained. The turn-on field of the randomly distributed nanotubes grown with the precursor of 3.5nm/3.5nm SiO_x/Fe decreases from 3.7 V/μm. to 2.2 V/μm due to the reduced density of the nanotubes.

The field-emission current density increased from $2.6x10^{-5}$ mA/cm^2 to $2.4x10^{-1}$ mA/cm^2 when the applied field was 4 V/μm, and the field emission current density reaches 2 $x10^{-3}$ mA/cm^2 as the applied field reached 6 V/μm. Besides, the best threshold field is about 5.32 V/μm with the precursor of 3.5 nm SiO_x on 3.5 nm Fe. Table 2-2 shows the summarized field-emission properties of the CNTs grown with different precursors.

2.3.2 Effect of Oxide Capping layer on Field Emission Properties of Carbon Nanotubes Grown by Thermal Chemical Vapor Deposition (TCVD)

Figure 2.10 shows the morphology of the deposited CNTs with the precursor of 5 nm Fe. The length of the deposited CNTs was approximately 4.9 μm. The CNTs was aligned and closely spaced, and only a few of them protruded above the CNT surface. The flat top of the CNTs tends to result in the screening effect of the electric field during cold cathode operation. The field enhancement factor therefore decreases and the CNT emitter has poor field-emission properties. Alternatively, the electric field tends to be larger in the edge region that has a relatively low density of CNTs than in the center of the film. The nonuniform electric field distribution near the CNTs also affects the field-emission current distribution. The field-emission current emitted from the edge region of the CNT film as the applied field exceeded the turn-on electric field and the center part of the CNTs started to emit under a higher applied field. A schematic illustration is shown in Fig. 2.4.

Figures 2.11(a) and 2.11(b) show SEM images of the deposited CNTs with the precursor of 1.5 nm/ 5 nm SiO_x/Fe. The density of nanotubes decreases obviously and the morphology of CNTs changes from aligned and closely spaced to curved and randomly distributed. The random distribution of the CNTs results in a lower density, which is good for electric field distribution.

SEM images of the deposited CNTs with the precursor of 7nm SiO_x/5nm Fe are shown in Figs 2-12(a)-2-12(b). The SEM image shows that the CNTs only grew on the edge of the precursor. No nanotubes were found in the center part of the precursor from the morphologies of the CNTs shown.

Figures 2.13(a) and 2.13(b) show SEM images of the deposited CNTs with the precursor of 15 nm/ 5 nm SiO_x/Fe. No nanotubes were found on most parts of the precursor except very few nanotubes were found on the edge of the precursor.

Figure 2-14 (a) shows the field-emission properties of the deposited CNTs with the precursor of 5nm Fe, 1.5nm SiO_x on 5nm Fe, 7nm SiO_x on 5nmFe nm and 15nm SiO_x on 5nm Fe. The corresponding F-N plots are shown in Fig. 2-14(b). The linearity of the F-N plot confirmed the field-emission phenomena. The turn-on electric field of the CNTs grown with 5 nm Fe was 3.8 V/μm, and the turn-on field of the CNTs grown with 1.5 nm SiO_x on 5 nm Fe and with 7nm SiO_x on 5nm Fe is 1.8 V/μm and 2 V/μm, respectively. The high turn-on field of the CNTs grown with 5 nm Fe is

attributed to the packed density of the nanotubes. When the applied field is 6 V/μm, the field-emission current density was 2.85mA/cm^2, 6.24mA/cm^2 and 14.6mA/cm^2 with the precursor of 5nm Fe, 1.5nm SiO_x on 5nm Fe, 7nm SiO_x on 5nm Fe nm, respectively. The threshold fields (Vth) are about 5.4 V/μm and 6.4 V/μm with the precursor of 7nm SiO_x on 5nm Fe and 1.5nm SiO_x on 5nm Fe nm, respectively. We do not find any field emission current of the CNTs grown with 15 nm SiO_x on 5 nm Fe because almost none of nanotubes are grown. Table 2-4 shows the summarized field-emission properties of the CNTs grown with different precursors.

2.4 Conclusions

The density control of CNTs achieved using a patterned precursor film with a thin SiO_x layer on a catalyst was proposed. The SEM images show that the morphology of the CNTs film grown by the MPCVD system can be modified using the precursor with a thin SiO_x film on a catalyst film. The MPCVD-grown CNTs tend to be randomly distributed for a SiO_x film thinner than 3.5 nm. A bilayered growth phenomenon of the nanotubes is discovered for the 7.5 nm SiO_x on 3.5 nm Fe patterned precursor film. For the precursor with a 15 nm SiO_x layer on 3.5 nm Fe, the nanotubes grow only in the edge region of the patterned precursor film. The difference in the morphologies of the grown CNTs with different precursors is

attributed to the variation in growth rate resulting from the thin SiO_x layer on the catalyst layer. The improvement in the field-emission properties of CNTs due to the modified surface morphology is also discovered. For the CNTs grown with the patterned precursor film containing 3.5 nm SiO_x on 3.5 nm Fe, the turn-on electric field reduces from 3.7 V/μm to 2.2 V/μm and the emission current density increases from $3.8x10^{-6}$ mA/cm^2 to $1.5x10^{-3}$m A/cm^2 at an applied electric field of 3.5 V/μm. Besides, the best threshold field is about 5.32 V/μm with the precursor of 3.5 nm SiO_x on 3.5 nm Fe.

The density control of TCVD grown CNTs achieved using a patterned precursor film with a thin SiO_x layer on a catalyst is proposed. The SEM images showed that the morphology of the CNTs film grown by the TCVD system can be modified using the precursor with a thin SiO_x film on a catalyst film. The TCVD-grown CNTs tend to be randomly distributed for a thinner SiO_x film. For the precursor with thicker SiO_x layer (larger than 7nm), the nanotubes grow only in the edge region of the patterned precursor film. Almost none of nanotubes grow when SiO_x layer larger than 15nm. Besides, we do not find the bilayer phenomena of nanotubes synthesized in TCVD. The difference in the morphologies of the grown CNTs with different precursors is attributed to the variation in growth rate resulting from the thin SiO_x layer on the catalyst layer. The improvement in the field-emission properties of CNTs due to the

modified surface morphology is also discovered. For the CNTs grown with the patterned precursor film containing 1.5 nm SiO_x on 5 nm Fe, the turn-on electric field reduces from 3.8 V/μm to 1.8 V/μm and the emission current density increases from 7 x 10^{-8} mA/cm^2 to 1.77mA/cm^2 at an applied electric field of 3.5 V/μm. For the CNTs grown with the patterned precursor film containing 7 nm SiO_x on 5 nm Fe, the turn-on electric field reduces from 3.8 V/μm to 2 V/μm and the emission current density increases from 7 x 10^{-8} mA/cm^2 to 2.1mA/cm^2 at an applied electric field of 3.5 V/μm. Besides, the threshold fields (Vth) are about 5.4 V/μm and 6.4 V/μm with the precursor of 7nm SiO_x on 5nm Fe and 1.5nm SiO_x on 5nm Fe nm, respectively.

The experimental results reveal that improved emission properties can be achieved by optimizing the density of CNTs using a suitable precursor film with an oxide capping layer on the catalyst layer.

Table 2-1 Experimental parameters of CNTs synthesized with SiO_x on Fe as precursor.

Sample #	A	B	C	D
Fe Thickness (nm)	3.5	3.5	3.5	3.5
SiO_x Thickness (nm)	0	3.5	7.5	15
Pretreatment	H_2 80 sccm, 35 torr, 1.2 kW, 10 min			
CNTs growth	H_2 80 sccm, N_2 80 sccm, CH_4 20 sccm, 35 torr, 1.2 kW, 10 min			

Table 2-2 Summarized field-emission properties of CNTs synthesized with SiO_x on Fe as precursors.

SiO_x/Fe (nm)	Turn-on field	Emission current density at 3.5 V/μm	Emission current density at 6 V/μm
0/3.5	3.7 V/μm	$3.8x10^{-6}$ mA/cm^2	$1.6x10^{-1}$ mA/cm^2
3.5/3.5	2.2 V/μm	$1.5x10^{-3}$mA/cm^2	2mA/cm^2
7.5/3.5	4.0 V/μm	-----	$5x10^{-2}$mA/cm^2
15/3.5	3.4 V/μm	$1.7x10^{-5}$ mA/cm^2	$2.2x10^{-1}$ mA/cm^2

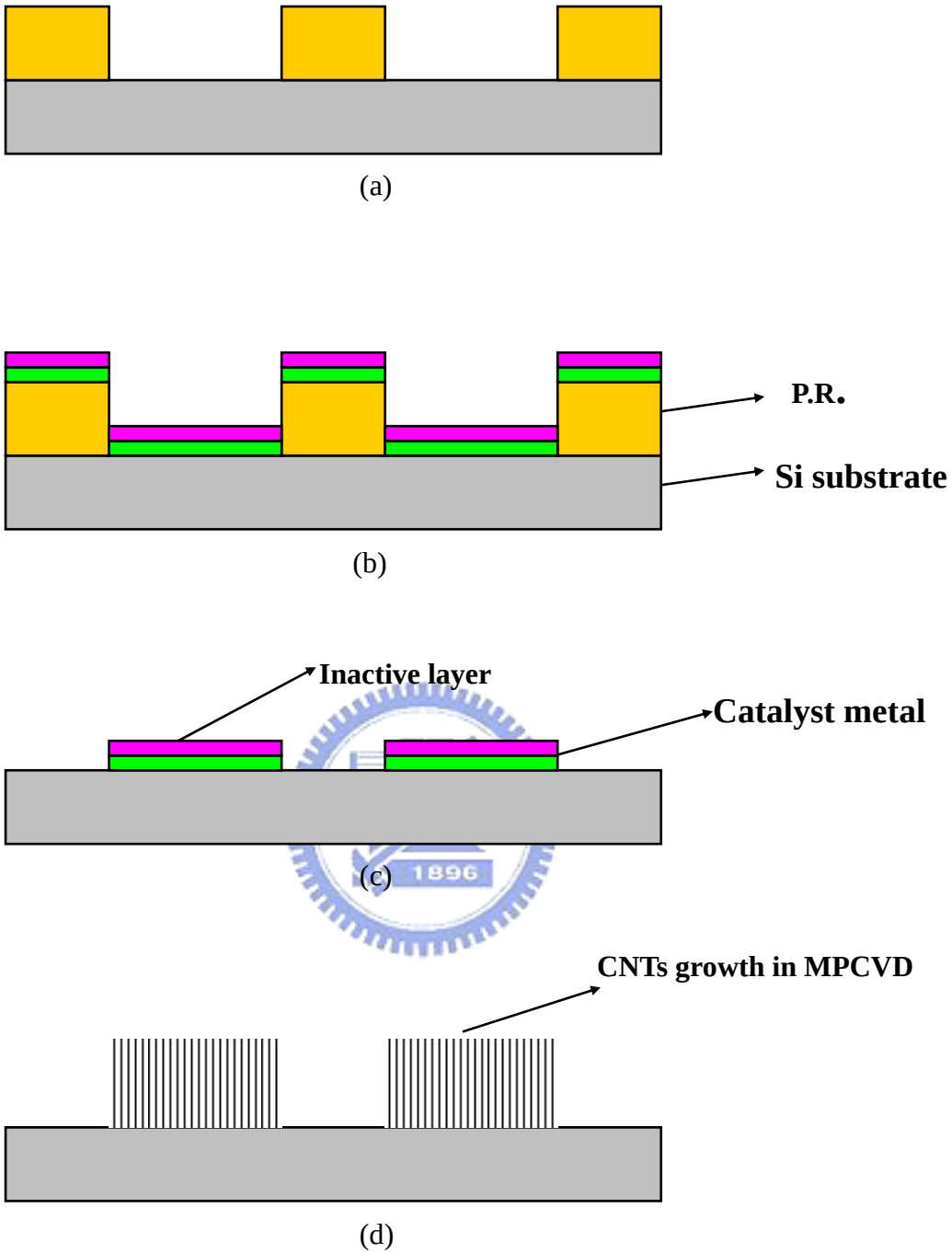

Figure2-1 Experimental procedures for CNTs synthesized using SiO_x on Fe as the precursor. (a) Patterned Si substrate by lithography, (b) deposition of catalyst layer and inactive layer, (c) photoresist lift-off and (d) carbon nanotube growth.

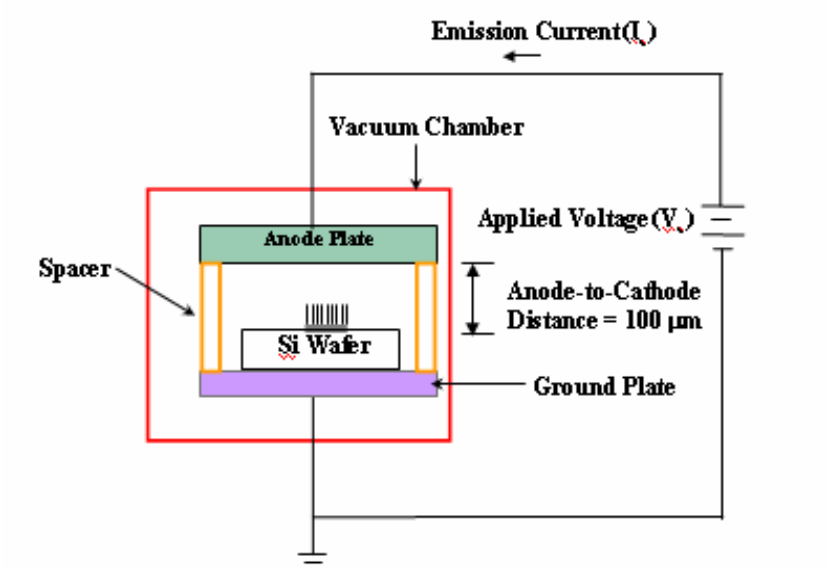

Figure2-2 Schematic diagram of high-vacuum field-emission measurement apparatus

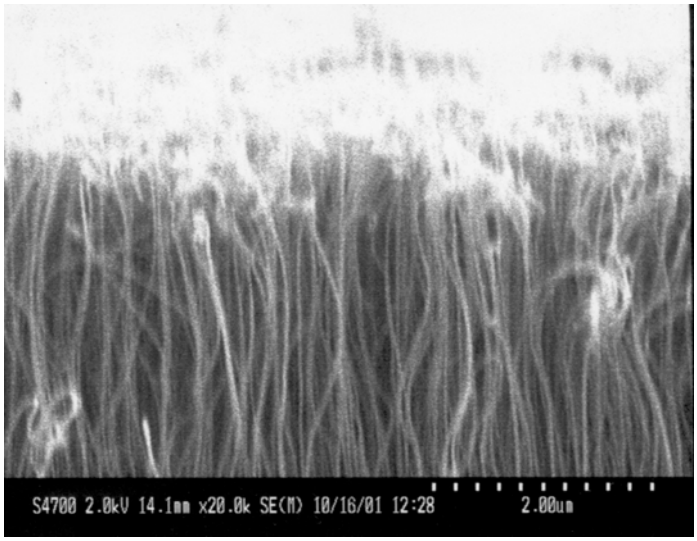

(a)

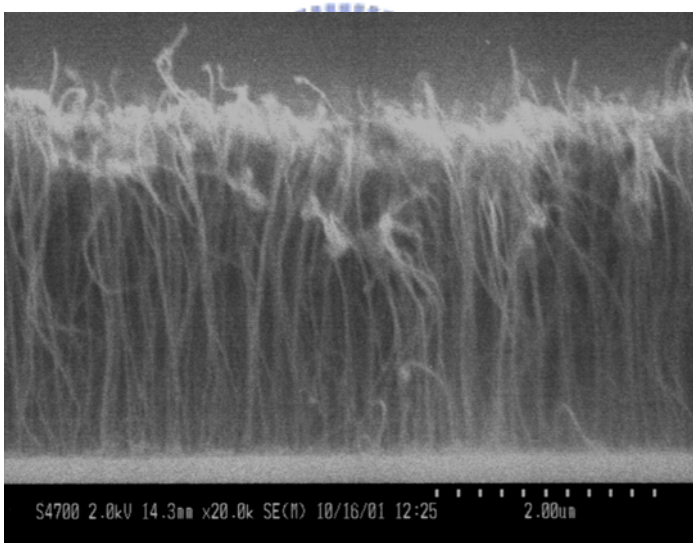

(b)

Figure2-3 SEM images of deposited CNTs with precursor of 3.5nm Fe.(a) 60^{o} top view and (b) cross sectional view.

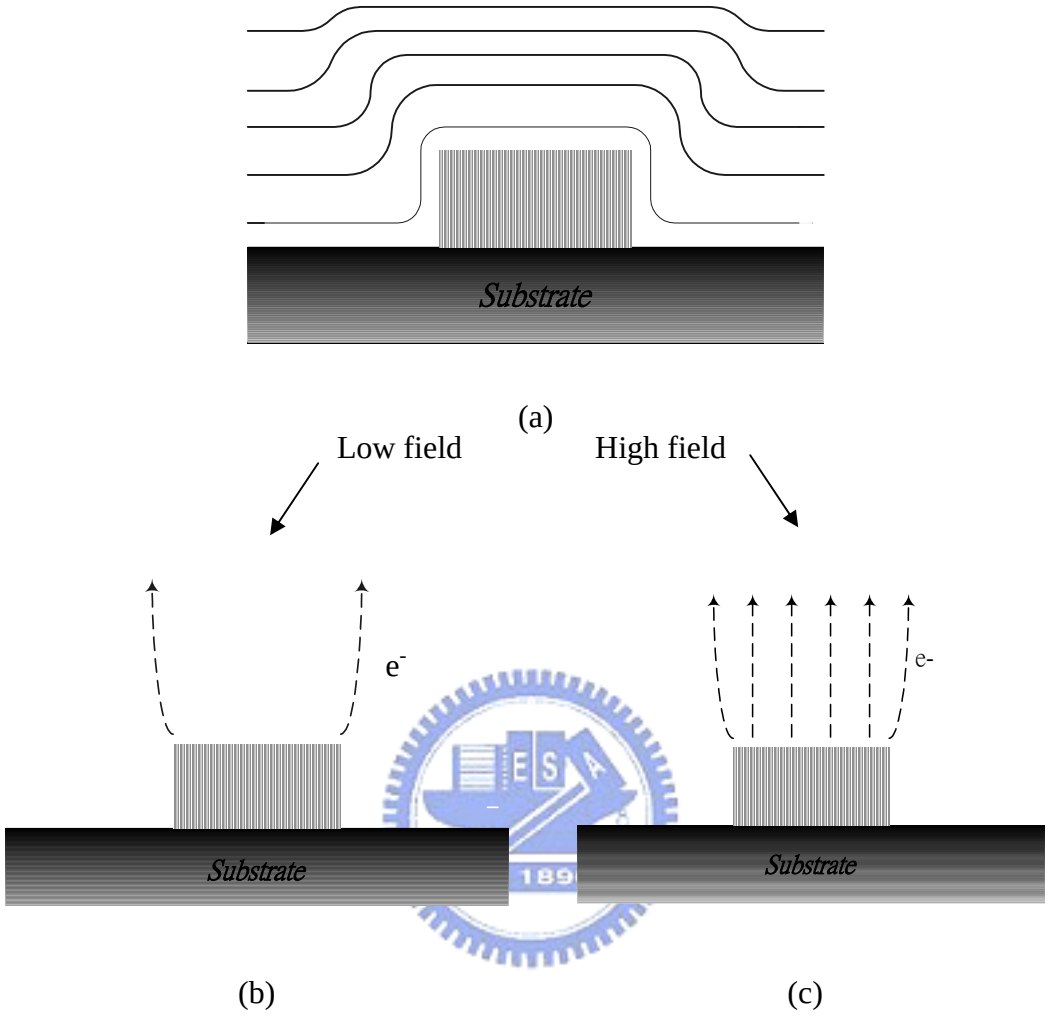

Figure2-4 Schematic illustration of electron field-emission vs applied electric field. (a) The static electric field of CNTs, (b) electrons emitted from edge region of CNT film as applied field exceeded turn-on electric field and (c) electrons emitted from center part of CNTs at higher applied field.

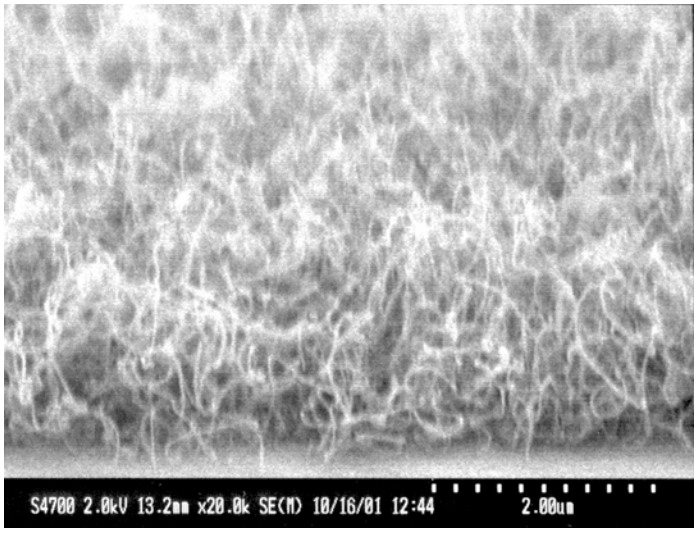

(a)

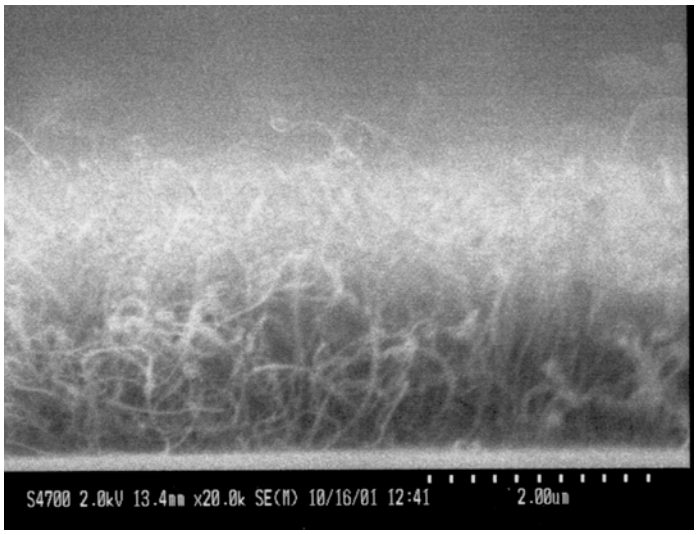

(b)

Figure2-5 SEM images of deposited CNTs with precursor of 3.5nm/3.5 nm SiO_x/Fe. (a) 60^o top view and (b) the cross-sectional view.

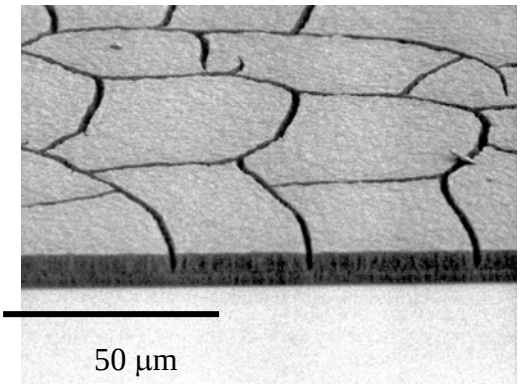

(a)

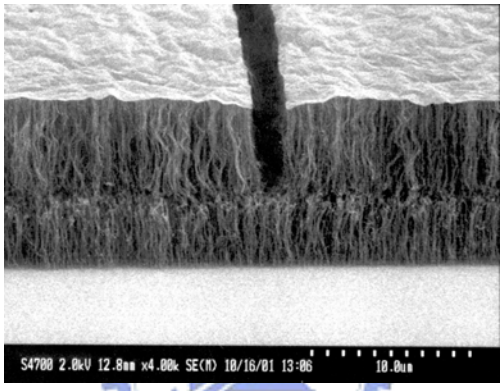

(b)

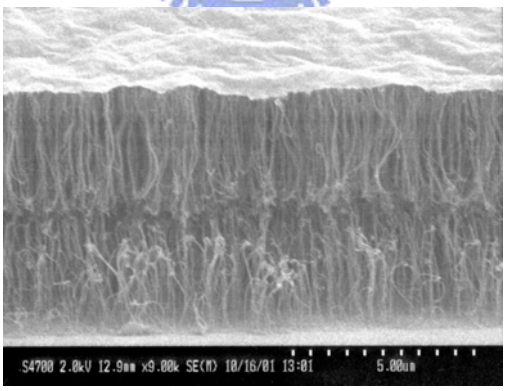

(c)

Figure2-6 SEM images of deposited CNTs with precursor of 7.5 nm/3.5 nm SiO_x/Fe. (a) Low magnification view, and (b)and (c) 60^o tilted views.

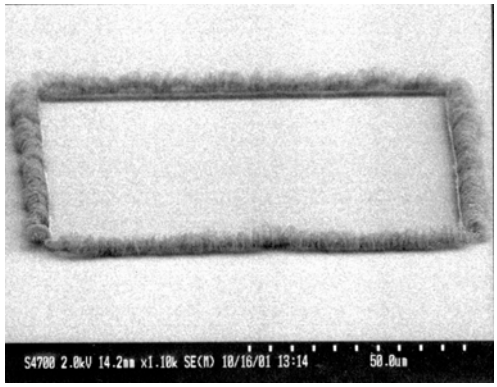

(a)

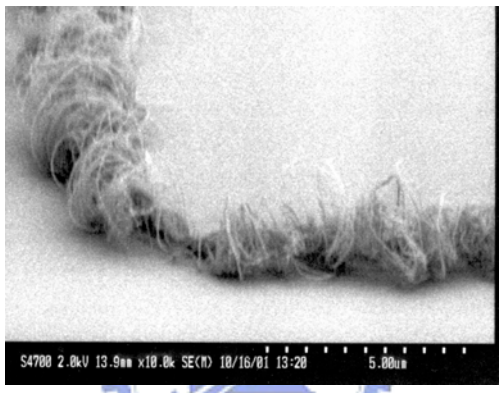

(b)

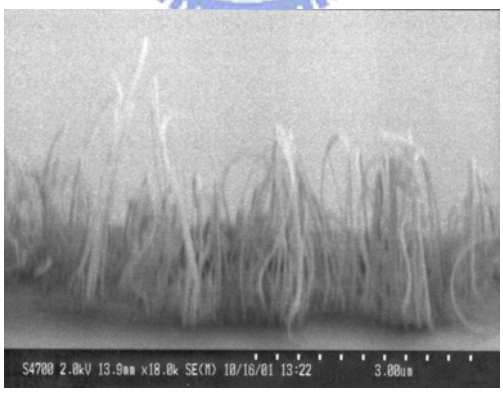

(c)

Figure2-7 SEM images of deposited CNTs with precursor of 15 nm/3.5 nm SiO_x/Fe. (a) Low magnified view, and (b)and (c) 60^o tilted views.